

Correlation Between DNA Double-Strand Break Distribution in 3D Genome and Ionizing Radiation-Induced Cell Death

Ankang Hu^{1,2}, Wanyi Zhou^{1,2}, Xiyu Luo³, Rui Qiu^{1,2,*}, and Junli Li^{1,2,*}

¹ Department of Engineering Physics, Tsinghua University, Beijing, China

² Key Laboratory of Particle & Radiation Imaging, Tsinghua University, Ministry of Education, Beijing, China

³ Institute of Fluid Physics, China Academy of Engineering Physics, Mianyang, China

*Authors to whom any correspondence should be addressed

Email: lijunli@mail.tsinghua.edu.cn and qiurui@tsinghua.edu.cn

Abstract. The target theory is the most classical hypothesis explaining radiation-induced cell death, yet the physical or biological nature of the “target” remains ambiguous. This study hypothesizes that the distribution of DNA double-strand breaks (DSBs) within the 3D genome is a pivotal factor affecting the probability of radiation-induced cell death. We propose that clustered DSBs in DNA segments with high interaction frequencies are more susceptible to leading to cell death than isolated DSBs. Topologically associating domain (TAD) can be regarded as the reference unit for evaluating the impact of DSB clustering in the 3D genome. To quantify this correlation between the DSB distribution in 3D genome and radiation-induced effect, we constructed a model that abstracts DNA interactions on the aspect of TADs. Utilizing track-structure Monte Carlo simulations, we calculated the incidence of each DSB case across a variety of radiation doses and linear energy transfers (LETs). Our simulation results suggest that clustered DSBs in a single TAD or distributed in TADs with frequent interaction are substantially more likely to induce cell death than isolated DSBs. These two DSB cases are also associated with cell death and the stochastic effects caused by high-LET irradiation. Our study highlights the critical role of the 3D genome structure in the underlying mechanisms of radiobiological effects. Our hypothesis contributes novel insights into the mechanisms governing radiobiological effects and provides a valuable reference for the development of mechanistic models capable of predicting cell survival under varying doses and LETs.

Keywords: ionizing radiation, DNA double-strand break, 3D Genome, topologically associating domain

Introduction

Radiotherapy is one of the main cancer treatment methods, where the induction of cell death via radiation plays a crucial role. The underlying mechanism by which radiation induces cell death forms the cornerstone of both the theory and practice of radiotherapy. The survival fraction of mammalian cells following irradiation at a specific dose is effectively captured by the survival fraction curve(1, 2). Characteristically, this curve exhibits a “shoulder” at lower dose ranges, transitioning to a near-linear relationship at higher dose ranges(3, 4). The survival fraction curve serves as the quintessential data backbone underpinning the clinical application of radiotherapy(5, 6).

Several theories have been proposed to elucidate the survival fraction curve, and corresponding

models have been developed based on these theories to predict cell death resulting from irradiation at specific doses and linear energy transfer (LET). The “target theory” is among the most seminal of these (7), positing that cells possess one or several critical “targets”; damage to these targets by irradiation, called “hit” or “lesion”, leads to cell death. The “target theory” underpins the vast majority of radiobiological theories.

The Linear-Quadratic (LQ) model(8) is the most widely utilized model in clinical practice, effectively quantifying the survival fraction within a range of several Gray. This model, as represented by Equation 1, suggests that the destruction of a target requires at least two lesions, which may be inflicted by either a single particle or multiple particles. The contribution of these lesions is quantified by the linear and quadratic terms within the model.

$$-\ln S = \alpha D + \beta D^2 \quad (1)$$

Where S represents the survival fraction, D denotes the radiation dose, and α and β are two intrinsic parameters. The ratio α/β , a critical parameter in radiotherapy, exhibits variability among different cell types, with typical values ranging from 2 Gy to 10 Gy.

“Structure determines function” is a fundamental principle in biology. The exact physical and biological entities of the “target” and “hit” remain an area of ongoing investigation.

Initially, the double-stranded DNA has been identified as the primary “target” with the strand breaks caused by radiation being considered as “damage”(9). The double-strand break (DSB) induced by a single radiation particle constitutes the first-order term in Eq 1. Conversely, the breakage of two opposite strands by separate particles, which subsequently combine to form a double-strand break, contributes to the second-order term. However, ample evidence indicates that the number of DSBs is directly proportional to the radiation dose(10–14), rather than adhering to the linear-quadratic formula as outlined in Equation 1. The occurrence of DSBs alone is insufficient to account for the formation of the cell survival curve.

In recent years, the larger aspect of DNA structure has come into focus as the key “target” in radiobiology. Researchers have differentiated double-strand breaks (DSBs) into two primary categories: isolated DSBs and complex DSBs(15–17). Isolated DSBs represent singular events, while complex DSBs are characterized by the occurrence of more than two DSBs within a defined “domain”, referred to as a “giant loop” in chromatin, which spans a region of 1-3 megabase pairs (Mbp) of DNA. Through the fitting of parameters against cell survival curve data, investigators have discovered that the probability of cell death resulting from complex DSBs is several orders of magnitude greater than that caused by isolated DSBs. Additionally, radiobiological effect models that account for high-linear energy transfer (LET), such as the microdosimetric kinetic (MK) model(18, 19) and the local effect model (LEM)(20), both propose the presence of a “domain” within the nucleus, approximately hundreds of nanometers in radius and encompassing about 2 Mbp of DNA (21). However, recent advancements in 3D genome mapping have revealed the intricate structure of chromosome folding within the nucleus, casting doubt on the concept of the “giant loop” as a distinct physical or biological entity within the cell(22, 23). Further research is imperative to delve into the specific domains that govern radiobiological effects, aiming to elucidate the complex interplay between radiation-induced damage and cellular response.

In this study, we hypothesize that the probability of DSBs leading to cell death is related to their distribution within the 3D genome. To quantify this hypothesis, we have developed a simplified model that takes into account the distribution of DSBs on the aspect of TADs. Subsequently, we investigate the correlation between the distribution of DSBs on the aspect of TAD and cell death

induced by irradiation at various doses and LETs using track-structure Monte Carlo simulations. Our hypothesis provides insights into the mechanisms of radiobiological effects and offers a valuable reference for developing mechanistic models that predict cell survival across a range of doses and LETs.

Materials and Methods

Hypothesis

In eukaryotic cells, chromatin is not randomly dispersed within the nucleus, rather, it is organized into a sophisticated hierarchical architecture, commonly referred to as the 3D genome(24, 25). Even genomic segments that are remote from each other in the linear sequence can engage in interactions through this 3D genomic structure, facilitating complex regulatory mechanisms. Numerous chromatin conformation capture assays, including Hi-C, have been utilized to explore the architecture of the 3D genome, revealing structural elements such as chromatin domains, compartments, and topologically associating domains (TADs)(26). Genes that exhibit frequent interactions are often in close spatial proximity and are associated with the same proteins, which can be detected through cross-linking in Hi-C experiments. The 3D genome structure governs the spatial proximity and interactions between DNA segments, and it is likely to be closely associated with the biological effects induced by radiation. Furthermore, TADs serve as functional units in the DNA damage response (27). For instance, they play a pivotal role in the loop extrusion process during double-strand break repair (28). Additionally, there may be a correlation between TADs and the effects induced by radiation.

We propose a hypothesis that DSBs that are clustered in the 3D genome, where the DNA segments containing DSBs exhibit high frequencies of interaction, the probability of incorrect repair leading to structural variations is significantly elevated compared to DSBs within segments that engage in infrequent interactions. As a result, the likelihood of cell death resulting from the clustered DSB scenario is considerably higher than that observed in the less frequently interacting segment scenario. Additionally, within the context of the clustered DSB scenario, the proximity of the two DNA segments in the genome is a critical factor: if the segments are in close genomic proximity, the occurrence of small-segment structural variation is more probable. Conversely, a large genomic distance between the segments is more likely to result in large-segment structural variations. We also suggest that the various types of structural variations may have differing probabilities of inducing cell death. Furthermore, TADs can be conceptualized as the reference unit for evaluating the impact of DSB clustering in the 3D genome on radiation-induced cellular responses. The diagram of our hypothesis is shown in Figure 1.

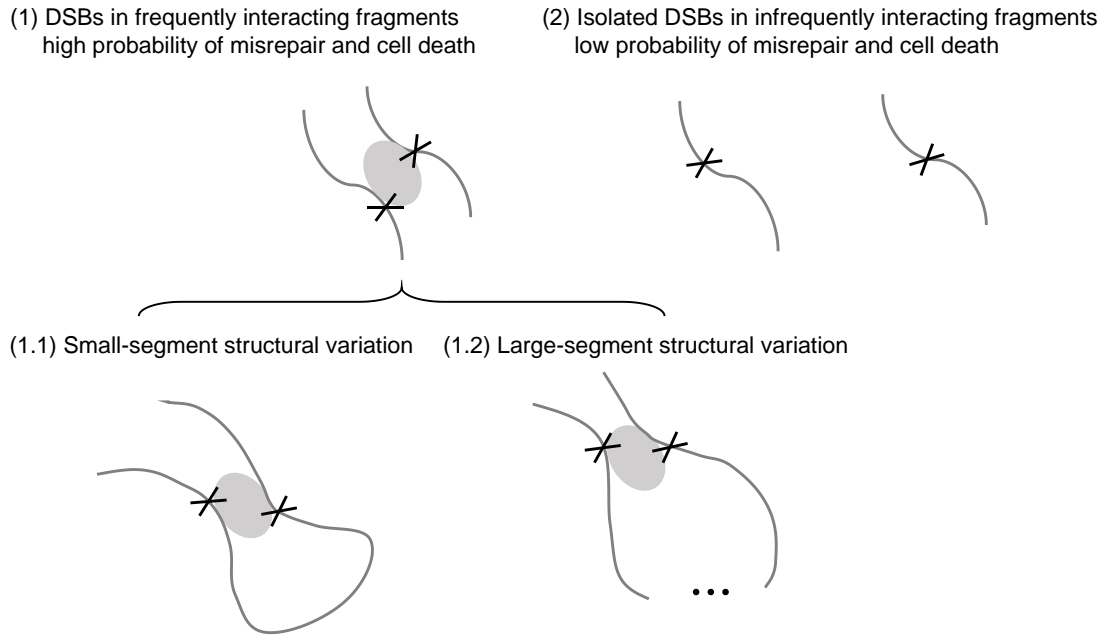


Figure 1. Diagram of our hypothesis

Quantifying the hypothesis through a mathematical model

To quantitatively assess our hypothesis, we have developed a simplified mathematical model. Establishing a quantitative relationship between interaction frequency and the probability of cell death is quite challenging. To tackle this challenge, we have classified the distribution of DSBs based on the aspect of TADs, as TADs are considered the fundamental units within the 3D genome structure(23, 29, 30). We have categorized the distribution of DSBs in the 3D genome into three distinct cases according to the interaction matrix obtained from Hi-C data, as depicted in Figure 2. For the sake of simplicity, our model assumes a uniform probability of outcomes within each scenario. In our classification system:

- Case 1 represents an isolated DSB, where a single TAD contains one DSB, and TADs that typically interact with this TAD are free of DSBs. This corresponds to scenario (2) in Figure 1.
- Case 2 is defined by clustered DSBs within a single TAD, where a single TAD harbors two or more DSBs. This corresponds to scenario (1.1) in Figure 1.
- Case 3 involves clustered DSBs across TADs that engage in frequent interactions (each TAD contains one DSB, and these TADs interact frequently with each other). This corresponds to scenario (1.2) in Figure 1.

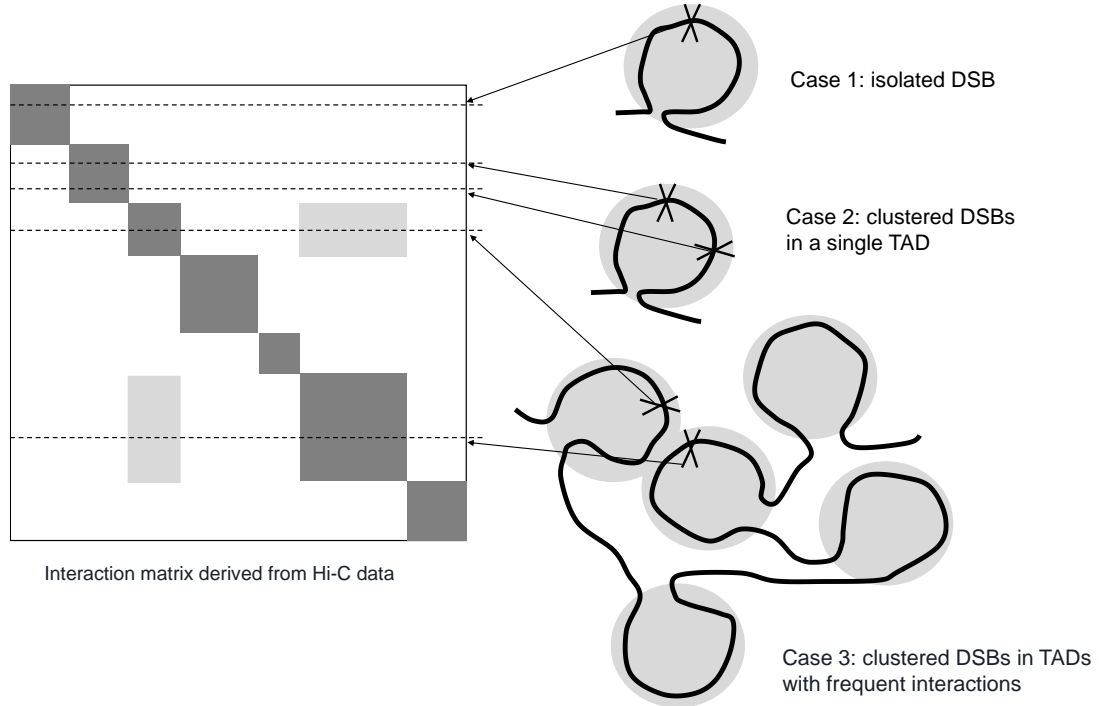


Figure 2. Three cases of DSBs in the model

The incidence of each case within a cell irradiated with a specific dose, D , can be denoted as $n_1(D)$ for Case 1, $n_2(D)$ for Case 2, and $n_3(D)$ for Case 3. Each case has a different probability of p_1 , p_2 , and p_3 , respectively, of resulting in a lethal event. The total number of lethal events can be determined using the formula provided in Equation 2.

$$n(D) = p_1 n_1(D) + p_2 n_2(D) + p_3 n_3(D) \quad (2)$$

Adopting the same assumptions employed in deriving the survival fraction model from the “target theory”, the number of lethal events is approximately Poisson-distributed. The survival fraction can then be computed using the formula provided in Equation 3.

$$S = \exp [-n(D)] \quad (3)$$

Consequently, we can forecast the survival fraction by the number of the three cases, utilizing the predictive formula detailed in Eq 4.

$$-\ln S = p_1 n_1(D) + p_2 n_2(D) + p_3 n_3(D) \quad (4)$$

The functions $n_1(D)$, $n_2(D)$ and $n_3(D)$ are determined by track-structure Monte Carlo simulations, which are elaborated in the subsequent section. The probabilities p_1 , p_2 , and p_3 are determined by specific cell types.

Track-structure Monte Carlo simulation study

We utilized the Geant4-DNA, a track-structure Monte Carlo simulation code previously developed, to compute the energy deposition points within the nucleus(31, 32). Subsequently, the data pertaining to these energy deposition points were imported into Python script for the analysis of DNA damage.

To study the distribution of DNA damage within the 3D genome, we employed a nuclear model that delineates topologically associating domains (TADs), as developed by Ingram et al. based on Hi-C data (33). This nuclear model represents TADs as spherical units, with the positions and radii of each sphere determined by a 3D genome modeling algorithm (22, 23). Additionally, the model provides information on the TADs that are known to interact frequently with a given TAD.

In the analysis of DNA damage, energy depositions that occur within topologically associating domains (TADs) are recorded. To translate these energy depositions into strand breaks, two conditions are implemented. First, a spatial sampling rate of 14.1% is applied to the TAD. Second, an energy range probability function is applied, which varies from 0 at 5 eV to 1 at 37.5 eV (12, 34, 35), indicating the likelihood of an energy deposition resulting in a strand break. An energy deposition is considered a strand break if it meets both conditions and is then randomly assigned to either strand 1 or strand 2 of the DNA double helix with equal probability. DSBs are defined as two or more strand breaks that occur on opposite strands and are within a distance of 3.2 nm or less from each other, which is approximately equivalent to 10 base pairs. All parameters for this setup are consistent with those used by Ingram et al. (33). The Density-Based Spatial Clustering of Applications with Noise (DBSCAN) algorithm is employed to analyze the distribution and clustering of DSBs. Then the incidences of three cases are counted for subsequent analysis. The Python scripts used for the analysis of DNA damage are available at the URL (https://github.com/hak1996/DSB_3D_genome).

We simulate 0.9 MeV electrons to represent low LET irradiation and C-12 ions with energies ranging from 2.98 MeV/u to 354.1 MeV/u to represent high LET irradiation. The relationship between the energy of the ion and the linear energy transfer (LET) is calculated based on the data provided by Furusawa et al. (36).

Acquisition of Cell Type-Specific Parameters

The simulation outcomes from electron irradiation are analyzed to derive the formulas for three distinct cases ($n_1(D)$, $n_2(D)$, and $n_3(D)$). We employ polynomial functions to approximate these formulas within the dose range. Subsequently, the probabilities of cell death for the three cases (p_1 , p_2 , p_3) are determined through fitting the survival fraction data of cells exposed to low LET radiation. Utilizing the probabilities obtained from low LET irradiation, we then calculate the survival fraction of cells subjected to C-12 ion irradiation.

Results and Discussions

Incidence of three cases irradiated by low LET radiation

The simulation results for electron irradiation are presented in Figure 3. We have set three different spatial sampling rates (p_{DNA}) to show the impact of these parameters on the outcomes. This parameter significantly influences the yield of DSBs and the occurrence of the three cases. The uncertainty associated with this parameter constitutes one of the main sources of uncertainty in our simulation and model.

The approximate formulas for describing the cases depicted in the figure are provided in Equation 5, with the corresponding parameters listed in Table 1.

$$\begin{aligned}
 n_{DSB} &= k_{DSB}D \\
 n_{case1} &= a_1D - b_1D^2 \\
 n_{case2,one} &= a_{2,1}D - b_{2,1}D^2 \\
 n_{case2,multi} &= b_{2,2}D^2 - c_{2,2}D^3 \\
 n_{case3} &= b_3D^2 - c_3D^3 + d_3D^4
 \end{aligned} \tag{5}$$

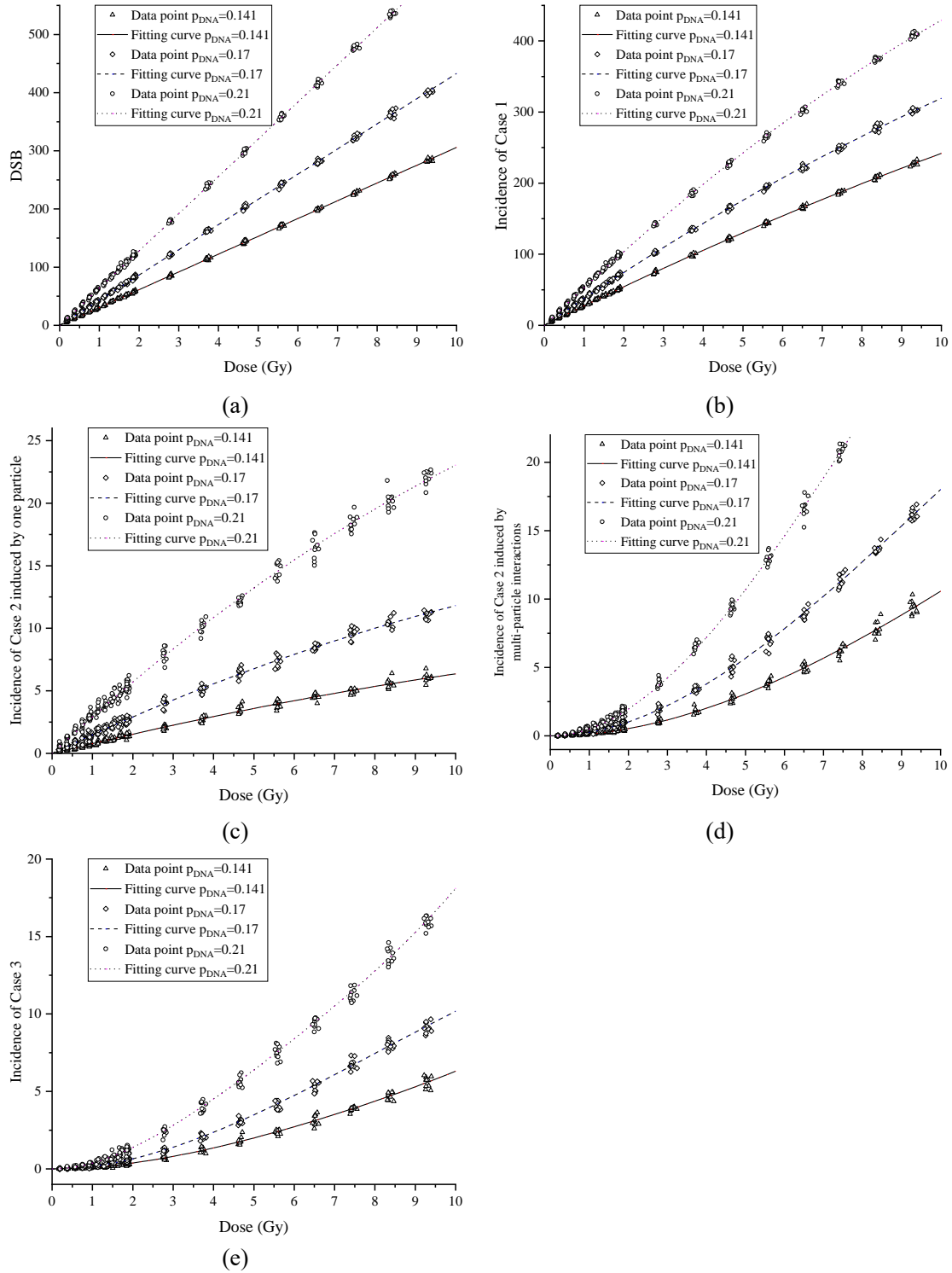


Figure 3. Incidence of events induced by electron irradiation. (a) DSB; (b) isolated DSB (case 1); (c) clustered DSB in a single TAD (case 2) induced by one particle; (d) clustered DSB in a single TAD (case 2) induced by multi particles; (e) clustered DSB in TADs with frequent interactions.

Table 1. Parameters of formulas describing the incidence of three cases

Parameters	$p_{DNA}=0.141$	$p_{DNA}=0.17$	$p_{DNA}=0.21$
k_{DSB}	30.59	38.49	54.09
a_1	27.85	0.6559	1.118

b_1	0.3665	1.527	2.988
$a_{2,1}$	0.8009	0.03458	0.06842
$b_{2,1}$	0.01646	0.2744	0.5342
$b_{2,2}$	0.1396	0.009434	0.02132
$c_{2,2}$	0.003387	0.1818	0.4258
b_3	0.1081	0.008832	0.04348
c_3	0.006831	8.33E-05	0.001901
d_3	0.0002325	38.49	54.09

Then the incidence of these cases can be calculated by Equation 6.

$$\begin{aligned}
 n_1(D) &= a_1D - b_1D^2 \\
 n_2(D) &= a_{2,1}D + (b_{2,2} - b_{2,1})D^2 - c_{2,2}D^3 \\
 n_3(D) &= b_3D^2 - c_3D^3 + d_3D^4
 \end{aligned} \tag{5}$$

The experimental results indicate that the DSB yield for low LET irradiation falls within the range of 30 to 50 Gy⁻¹ (12, 14, 33). Our results are in agreement with the reported DNA DSB yields for low LET radiation.

The occurrence of the second term in case 2, which is induced by multiple particles, and the incidence of case 3 may account for the “shoulder” observed in the survival fraction curve at low doses. As the dose increases, the incidences of case 2 and case 3 tend to follow straight lines, corresponding to the “straight line” portion of the survival fraction curve observed at high doses.

Probability of cell death induced by the three cases

Utilizing the formulas provided in Equation 5 and the parameter $p_{DNA}=0.141$ as specified in Table 1, we have fitted the survival fractions for different cell types to determine the probability of cell death caused by the three respective cases (p_1 , p_2 and p_3). The resulting probabilities are presented in Table 2. The cell survival fraction data for samples No. 1 through 16 were obtained by Suzuki et al. (37). Samples No. 17 and 18 were sourced from the study by Furusawa et al. (36). Sample No. 19 was derived from the research by Elkind and Sutton (2), sample No. 20 was obtained from the study by Puck and Marcus (1), sample No. 21 was obtained from the study by Bronk et al. (38).

Table 2. Probability of cell death induced by the three cases through fitting and goodness of fitting

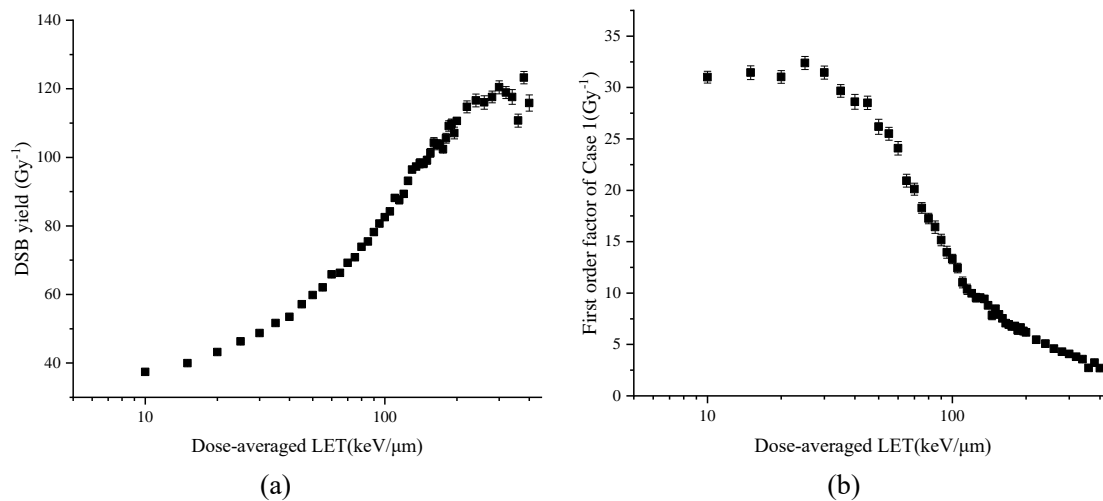
No.	Cell type	p_1	p_2	p_3	R^2
1	NB1RGB	0.01440	5.07E-11	0.8017	0.9993
2	HFL-III	0.001538	0.4271	0.1686	0.9993
3	LC-1 sq	4.63E-09	0.3353	0.9999	0.9971
4	A-549	7.27E-13	1.00E-12	0.8131	0.9946
5	C32TG	0.007442	0.009226	0.5901	0.9997
6	Marcus	0.002965	2.41E-07	0.8464	0.9976
7	U-251 MG (KO)	7.35E-12	2.22E-14	0.9847	0.9630
8	SK-MG-1	0.001539	6.17E-07	0.8501	0.9966
9	KNS-89	1.53E-12	0.1006	1.000	0.9893
10	KS-1	0.02298	2.22E-14	0.783859	0.9974
11	A-172	0.001562	0.2338	1.000	0.9820
12	ONS-76	2.35E-08	0.1071	0.9999	0.9810

13	KNS-60	1.15E-12	2.22E-14	0.7334	0.9939
14	Becker	8.47E-12	0.08776	0.2227	0.9965
15	T89G	5.18E-08	2.23E-14	0.7674	0.9982
16	SF126	0.005126	3.86E-11	0.9907	0.9972
17	V79	0.003685	0.07019	0.2501	0.9997
18	HSG	0.001666	0.3554	0.2356	0.9995
19	Hela	0.01688	0.01690	1.000	0.9942
20	Chinese hamster	0.008389	2.22E-14	0.6856	0.9958
21	H460	7.89E-9	0.163521	0.9999	0.9865

The results indicate that the probabilities p_2 and p_3 are typically much greater than p_1 , suggesting that DSBs within DNA segments that engage in frequent interactions are much more likely to result in cell death.

Correlation between DSB distribution and cell death induced by high LET irradiation

The simulation outcomes for C-12 ions with varying LET values are depicted in Figure 4. Since the incidence of double-strand breaks (DSBs) is directly proportional to the dose, we have chosen to display the yield of DSBs. For the incidence of case 1 and the incidence of case 2 caused by one particle, we present the factors associated with the first-order terms. Regarding the incidence of case 2 resulting from multiple particles, due to the high statistical error associated with the parameters, we instead show the incidence at a dose of 1 Gy. For the incidence of case 3, due to the high statistical errors of parameters, we display the incidence at both 1 Gy and 4 Gy.



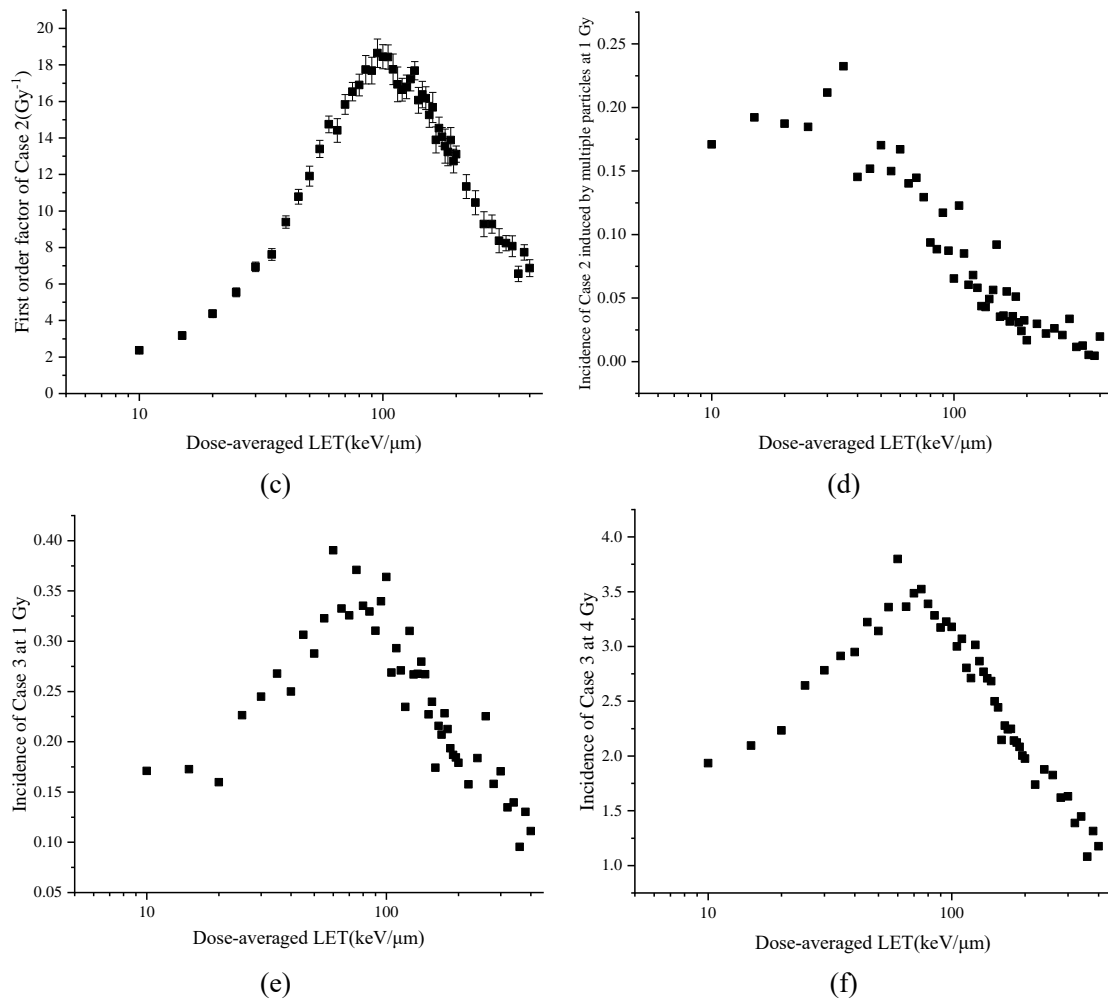


Figure 4. Simulation results of C-12 ions. (a) yield of DSB; (b) first-order factor of case 1; (c) first-order factor of case 2 induced by one particle; (d) incidence of case 2 induced by multiple particles at 1 Gy; (e) incidence of case 3 at 1 Gy; (f) incidence of case 3 at 4 Gy.

The results indicate that the yield of double-strand breaks (DSBs) increases with the increment of linear energy transfer (LET), suggesting that the mere number of DSBs is insufficient to fully explain radiation-induced cell death. Empirical Relative Biological Effectiveness (RBE) data, indicates that RBE reaches a peak when the LET is approximately 100 keV/μm (39). In comparison to the single-particle-induced case 2 for high LET irradiation, the contribution of case 2 induced by multiple particles is negligible. The yield of case 2 reaches its maximum at an LET of around 100 keV/μm, in correspondence with the empirical RBE data. The incidence of case 3 exhibits a peak at LET values in the tens of keV/μm range.

These results suggest a correlation between the distribution of DSBs within the 3D genome structure and the induction of cell death by high LET irradiation.

Moreover, by utilizing the probabilities of cell death resulting from the three cases (as obtained from low LET irradiation), we have calculated the survival fraction for C-12 ion irradiation. The calculated survival fractions of V79 cells are presented and compared with the experimental results provided by Furusawa et al. (36) in Figure 5. The calculated RBE at 10% and 50% survival fraction of H460 cells are presented and compared with experimental results provided by Bronk et al. (38) in Figure 6.

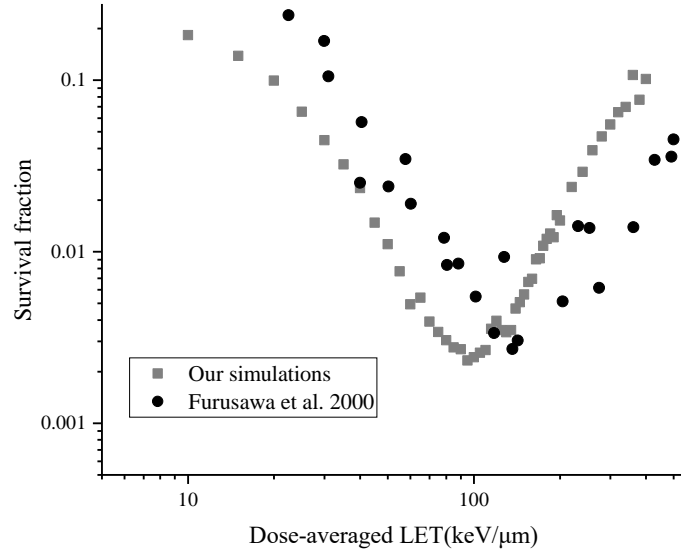


Figure 5. Comparison between the survival fraction of V79 cells calculated using our simulation and the experimental results obtained by Furusawa et al.

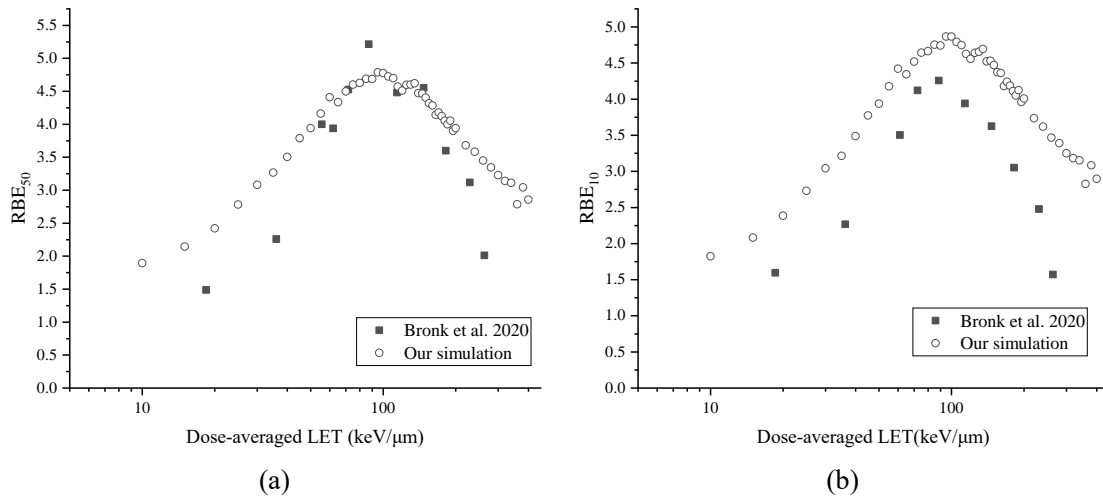


Figure 6. Comparison between the RBE of H460 cells calculated using our simulation and the experimental results obtained by Bronk et al. (a) RBE at 50% survival fraction; (b) RBE at 10% survival fraction.

Our simulation results exhibit a trend that aligns with the experimental data. This alignment also suggests a correlation between the spatial distribution of DSBs within the 3D genome structure and the subsequent induction of cell death by high LET irradiation.

Correlation between DSB distribution and radiation quality

Radiological risk is closely associated with radiation-induced DNA damage. Our hypothesis proposes that DSBs occurring in DNA segments that frequently interact are more likely to result in misrepair. We further speculate that the distribution of DSBs within the 3D genome structure is also related to radiation-induced stochastic effects. In the low dose range that is of concern in radiation protection, the incidence of case 3 and case 2 induced by multiple particles can be overlooked. We have presented the first-order factor of case 2, induced by a single particle, in

Figure 7, along with the radiation quality recommended by ICRP 92 (40) and as derived by Borak et al. (41), to show their correlations.

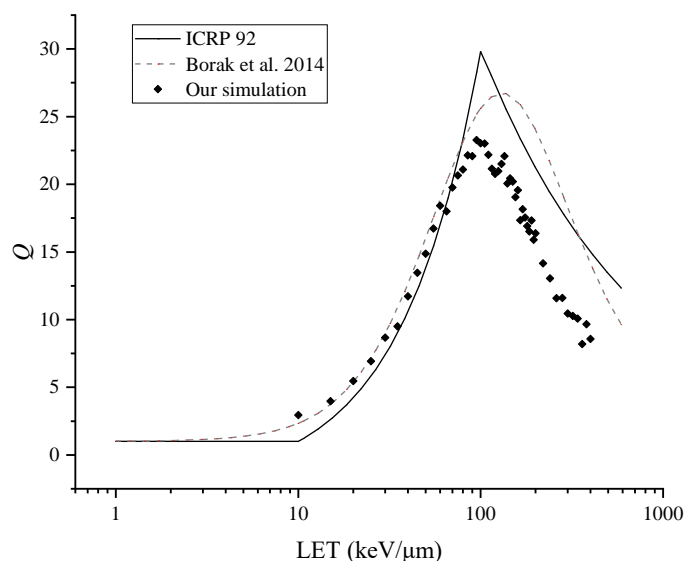


Figure 7. Correlation between the yield of clustered DSBs in a single TAD and radiation quality.

Discussion on the “target” and “domain”

The identification of the physical and biological entities referred to as “targets” or “domains” is a pivotal process in unraveling the mechanisms underlying radiobiological cell death. Numerous phenomena suggest that DNA double strands, in isolation, do not fully encapsulate the concept of a “target” or “domain.” Consequently, theories founded solely on this premise are inadequate in accurately predicting cell survival fractions.

Recent theories have proposed the existence of a “domain” at a larger scale, with fitting results suggesting a diameter of approximately 500 nm for these domains (15, 16). However, this scale does not correspond to any known cellular structure. The typical diameter of a TAD is only about 200 nm (42), which is roughly half the size of the proposed “domain”. This discrepancy suggests that the concept of “targets” or “domains” as distinct physical or biological entities may be oversimplified. Besides the domain, e.g. TAD, the critical factor could be the interaction between damaged DNA segments and their distance in the genome. TADs and other architectural elements within the 3D genome are indeed characterized by the interactions among DNA segments. Therefore, a comprehensive model of radiobiological response should encompass the impact of these interactions and the spatial arrangement of DNA on radiobiological outcomes, rather than focusing solely on specific, fixed-size targets. However, due to the potentially complex relationship between the frequency of DNA segment interactions and cell death, our study employed a simplified model. In this model, the interactions between DNA segments are elegantly captured by representing them with TADs and those TADs that engage in frequent interactions.

Discussion on the motivation and limitations of our study

The objective of our study is to elucidate the correlation between the distribution of DNA within the 3D genome structure and radiation-induced cell death, rather than to develop a model for predicting cell survival at specific doses and LET values. The causal relationship has not yet been experimentally validated. There is no imperative to establish a new model to predict exact cell

survival fractions by modifying the parameters with clear physical or biological relevance in this study. The model developed in this study is solely intended to demonstrate the quantitative correlation; we do not endeavor to adjust the parameters to conform to experimental data.

Beyond the simplification of DNA segment interactions to TADs and the assumption of a uniform probability of inducing cell death for all conditions that are simplified to one case in our study, the intrinsic uncertainties associated with track-structure Monte Carlo simulations and nuclear models introduce significant uncertainty into the estimated quantities of DNA damage. As evidenced in the preceding sections, the parameters within the simulation have a profound influence on the results, yet the precise values for these parameters remain elusive. Our simulation is capable of illustrating general trends rather than delivering exact numerical values. Additionally, the experimental data on cell survival fractions often contains large uncertainty, which in turn constrains the derivation of a definitive quantitative relationship for accurately predicting cell survival fractions.

Conclusion

This study advances the hypothesis that the distribution of DSBs within the 3D genome is a predominant factor influencing radiation-induced cell death. We suggest that clustered DSBs in DNA segments with high interaction frequencies are more likely to result in cell death than isolated DSBs. TAD can be regarded as the reference unit for evaluating the impact of DSB clustering in the 3D genome. To study this correlation quantitatively, we developed a simplified model. In this model, DSBs are categorized into three cases based on their distributions on the aspect of TADs. The incidences of each case of DSB induced by irradiation at various doses and LETs were calculated using track-structure Monte Carlo simulations. The results indicate that DSB clusters within a single TAD (case 2) or in TADs with frequent interactions (case 3) are significantly more probable to trigger cell death than isolated DSBs (case 1). The incidences of cases 2 and 3 are also correlated with cell death and the stochastic effects induced by high-LET irradiation. Our research underscores the importance of the 3D genome structure in the mechanisms of radiobiological effects. Furthermore, it provides insight for subsequent studies investigating the role of the 3D genome and for the development of models that predict cell survival and RBE based on underlying mechanisms.

Acknowledgments

This work was supported by the National Key Research and Development Program of China (Grant No. 2024YFA1014103), the National Natural Science Foundation of China (Grant No. 12405359) and the Postdoctoral Fellowship Program of Chinese Postdoctoral Science Foundation under Grant Number GZB20240342.

References

1. Puck TT, Marcus PI. ACTION OF X-RAYS ON MAMMALIAN CELLS. *Journal of Experimental Medicine*. 1956;103(5):653–66.
2. Elkind MM, Sutton H. X-Ray Damage and Recovery in Mammalian Cells in Culture. *Nature*.

1959;184(4695):1293–5.

3. Cohen–Jonathan E, Bernhard EJ, McKenna WG. How does radiation kill cells? *Current Opinion in Chemical Biology*. 1999;3(1):77–83.
4. Liu R, Higley KA, Swat MH, Chaplain MAJ, Powathil GG, Glazier JA. Development of a coupled simulation toolkit for computational radiation biology based on Geant4 and CompuCell3D. *Phys Med Biol*. 2021;66(4):045026.
5. Hall EJ, Giaccia AJ. *Radiobiology for the radiologist*. 8th ed. Lippincott Williams & Wilkins; 2018.
6. Manganaro L, Russo G, Bourhaleb F, et al. ‘Survival’: a simulation toolkit introducing a modular approach for radiobiological evaluations in ion beam therapy. *Phys Med Biol*. 2018;63(8):08NT01.
7. Nomiya T. Discussions on target theory: past and present. *Journal of Radiation Research*. 2013;54(6):1161–3.
8. McMahon SJ. The linear quadratic model: usage, interpretation and challenges. *Phys Med Biol*. 2018;64(1):01TR01.
9. Chadwick KH, Leenhouts HP. A molecular theory of cell survival. *Phys Med Biol*. 1973;18(1):78.
10. Schneider U, Vasi F, Besserer J. The probabilities of one- and multi-track events for modeling radiation-induced cell kill. *Radiat Environ Biophys*. 2017;56(3):249–54.
11. Belov OV, Krasavin EA, Lyashko MS, Batmunkh M, Sweilam NH. A quantitative model of the major pathways for radiation-induced DNA double-strand break repair. *J Theor Biol*. 2015;366:115–30.
12. Friedland W, Dingfelder M, Kundrat P, Jacob P. Track structures, DNA targets and radiation effects in the biophysical Monte Carlo simulation code PARTRAC. *Mutat Res*. 2011;711(1–2):28–40.
13. Forster JC, Douglass MJJ, Phillips WM, Bezak E. Monte Carlo Simulation of the Oxygen Effect in DNA Damage Induction by Ionizing Radiation. *Radiat Res*. 2018;190(3):248–61.
14. de Lara CM, Hill MA, Jenner TJ, Papworth D, Neill PO. Dependence of the Yield of DNA Double-Strand Breaks in Chinese Hamster V79-4 Cells on the Photon Energy of Ultrasoft X Rays. *Radiation Research*. 2001;155(3):440–8.
15. Liew H, Tessonnier T, Mein S, et al. Robustness of carbon-ion radiotherapy against DNA damage repair associated radiosensitivity variation based on a biophysical model. *Medical Physics*. 2024;51(5):3782–95.
16. Friedrich T, Scholz U, Elsasser T, Durante M, Scholz M. Calculation of the biological effects of ion beams based on the microscopic spatial damage distribution pattern. *Int J Radiat Biol*. 2012;88(1–2):103–7.
17. Liew H, Meister S, Mein S, et al. Combined DNA Damage Repair Interference and Ion Beam Therapy: Development, Benchmark, and Clinical Implications of a Mechanistic Biological Model. *International Journal of Radiation Oncology*Biophysics*. 2022;112(3):802–17.
18. Hawkins RB. A microdosimetric-kinetic model of cell death from exposure to ionizing radiation of any LET, with experimental and clinical applications. *International Journal of Radiation Biology*. 1996;69(6):739–55.
19. Chen Y, Li J, Li C, Qiu R, Wu Z. A modified microdosimetric kinetic model for relative biological effectiveness calculation. *Phys Med Biol*. 2017;63(1):015008.

20. Elsasser T, Scholz M. Cluster effects within the local effect model. *Radiat Res.* 2007;167(3):319–29.
21. Bordieri G, Missiaggia M, Cartechini G, et al. Validation of the generalized stochastic microdosimetric model (GSM²) over a broad range of LET and particle beam type: a unique model for accurate description of (therapy relevant) radiation qualities. *Phys Med Biol.* 2024;70(1):015005.
22. Paulsen J, Sekelja M, Oldenburg AR, et al. Chrom3D: three-dimensional genome modeling from Hi-C and nuclear lamin-genome contacts. *Genome Biology.* 2017;18(1):21.
23. Szabo Q, Jost D, Chang J-M, et al. TADs are 3D structural units of higher-order chromosome organization in *Drosophila*. *Science Advances.* 2018;4(2):eaar8082.
24. Nichols MH, Corces VG. Principles of 3D compartmentalization of the human genome. *Cell Rep.* 2021;35(13):109330.
25. Rowley MJ, Corces VG. Organizational principles of 3D genome architecture. *Nat Rev Genet.* 2018;19(12):789–800.
26. Bienko M. How Hi-C ignited the era of 3D genome biology. *Nat Rev Genet.* 2023;24(7):418–418.
27. Andriotty M, Wang C-KC, Kapadia A, McCord RP, Agasthya G. Integrating chromosome conformation and DNA repair in a computational framework to assess cell radiosensitivity*. *Phys Med Biol.* 2024;69(24):245017.
28. Arnould C, Rocher V, Finoux A-L, et al. Loop extrusion as a mechanism for formation of DNA damage repair foci. *Nature.* 2021;590(7847):660–5.
29. Chang LH, Ghosh S, Noordermeer D. TADs and Their Borders: Free Movement or Building a Wall? *J Mol Biol.* 2020;432(3):643–52.
30. Szabo Q, Bantignies F, Cavalli G. Principles of genome folding into topologically associating domains. *Science Advances.* 2019;5(4):eaaw1668.
31. Bernal MA, Bordage MC, Brown JMC, et al. Track structure modeling in liquid water: A review of the Geant4-DNA very low energy extension of the Geant4 Monte Carlo simulation toolkit. *Physica Medica.* 2015;31(8):861–74.
32. Li JL, Li CY, Qiu R, et al. DNA Strand Breaks Induced by Electrons Simulated with Nanodosimetry Monte Carlo Simulation Code: Nasic. *Radiat Prot Dosim.* 2015;166(1–4):38–43.
33. Ingram SP, Henthorn NT, Warmenhoven JW, et al. Hi-C implementation of genome structure for in silico models of radiation-induced DNA damage. *PLOS Computational Biology.* 2020;16(12):e1008476.
34. Friedland W, Jacob P, Kundrat P. Stochastic simulation of DNA double-strand break repair by non-homologous end joining based on track structure calculations. *Radiat Res.* 2010;173(5):677–88.
35. Friedland W, Kundrat P, Becker J, Eidemuller M. Biophysical Simulation Tool Partrac: Modelling Proton Beams at Therapy-Relevant Energies. *Radiat Prot Dosimetry.* 2019;186(2–3):172–5.
36. Furusawa Y, Fukutsu K, Aoki M, et al. Inactivation of Aerobic and Hypoxic Cells from Three Different Cell Lines by Accelerated ³He-, ¹²C- and ²⁰Ne-Ion Beams. *Radiation Research.* 2000;154(5):485–96.
37. Suzuki M, Kase Y, Yamaguchi H, Kanai T, Ando K. Relative biological effectiveness for cell-killing effect on various human cell lines irradiated with heavy-ion medical accelerator in

- Chiba (HIMAC) carbon-ion beams. *Int J Radiat Oncol Biol Phys*. 2000;48(1):241–50.
38. Bronk L, Guan F, Patel D, et al. Mapping the Relative Biological Effectiveness of Proton, Helium and Carbon Ions with High-Throughput Techniques. *Cancers*. 2020;12(12):3658.
39. Chang DS, Lasley FD, Das IJ, Mendonca MS, Dynlacht JR. Oxygen Effect, Relative Biological Effectiveness, and Linear Energy Transfer. In: Chang DS, Lasley FD, Das IJ, Mendonca MS, Dynlacht JR, editors. *Basic Radiotherapy Physics and Biology*. Cham: Springer International Publishing; 2021. p. 255–60. [cited 2024 Dec 24] Available from: https://doi.org/10.1007/978-3-030-61899-5_24.
40. Valentin J. Relative biological effectiveness (RBE), quality factor Q, and radiation weighting factor wR): ICRP Publication 92. *Ann ICRP*. 2003;33(4):1–121.
41. Borak TB, Heilbronn LH, Townsend LW, McBeth RA, de Wet W. Quality factors for space radiation: A new approach. *Life Sciences in Space Research*. 2014;1:96–102.
42. Szabo Q, Jost D, Chang JM, et al. TADs are 3D structural units of higher-order chromosome organization in *Drosophila*. *Sci Adv* [Internet]. 2018;4(2) doi:ARTN eaar8082 10.1126/sciadv.aar8082.